Synthesis, structural characterization, Hirshfeld surface analysis, and theoretical investigations of *bis*(benzene-1,2-dicarboxylato)*bis*(4-methylbenzohydrazide)zinc

C. Balakrishnan, M. Manonmani, S. P. Meenakshisundaram & R. M. Sockalingam

Taylor & Francis
Taylor & Francis Group

Check for updates

Synthesis, structural characterization, Hirshfeld surface analysis, and theoretical investigations of *bis*(benzene-1,2-dicarboxylato)*bis*(4-methylbenzohydrazide)zinc

C. Balakrishnan, M. Manonmani, S. P. Meenakshisundaram, and R. M. Sockalingam

Department of Chemistry, Annamalai University, Annamalainagar, Tamilnadu, India

ABSTRACT

Single crystals of bis(benzene-1,2-dicarboxylato)bis(4-methylbenzohydrazide)zinc (ZPTH), a novel Zn(II) complex of phthalic acid and hydrazide, were grown from aqueous solution by slow evaporation solution growth technique. The compound $C_{32}H_{30}N_4O_{10}Zn$ crystallizes in triclinic system with centrosymmetric space group Pī. Its structure is built up from octahedral (ZnO_4N_2) linked to each other through the phthalate and hydrazide groups. The good crystallinity of the as-grown specimen is confirmed by the powder X-ray diffraction pattern. The band gap energy is estimated using diffuse reflectance data by the application of Kubelka–Munk algorithm. ZPTH exhibits fluorescent emission at 401 nm in the solid state at room temperature. Theoretical calculations were performed using density functional theory (DFT) method. Experimental observations are well supported by theoretical studies.

GRAPHICAL ABSTRACT
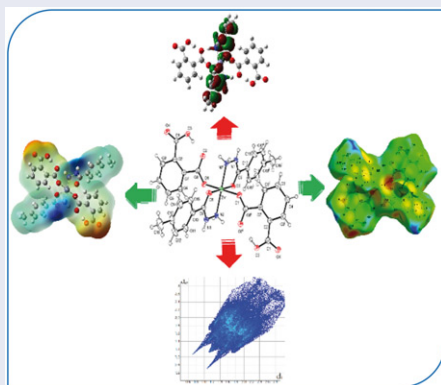
CONTACT R. M. Sockalingam ✉ rmslingam@gmail.com ⊡ Department of Chemistry, Annamalai University, Annamalainagar 608 002, Tamilnadu, India.

Color versions of one or more of the figures in the article can be found online at www.tandfonline.com/gmcl.

Supplemental data for this article can be accessed on the publisher's website.

Introduction

The chemistry of mixed organic–inorganic architectures has received much attention due to the assembly of metal-centered building units with organic linkers [1]. This type of metal-organic frameworks have promising applications in the area of catalysis [2] and biological activity [3]. Phthalate anion is a well-known piezoelectric, pyroelectric, and electro-optic versatile ligand able to chelate metal ions leading to the formation of polynuclear and low-dimensional systems [4,5].
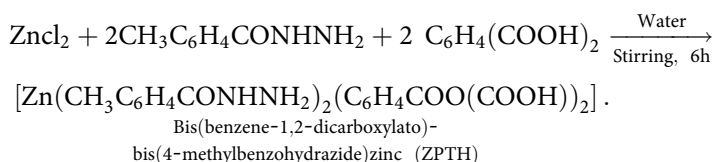
Hydrazides are potential chelating agents and form noncovalent interactions. Transition metal complexes with hydrazides and hydrazones, mono- and dinuclear 2,6-diacetylpyridine hydrazone copper [6], unsymmetric bishydrazide [7], zinc(II) complex with methanesulfonylhydrazine [8], aqua(4-methyl- 1-naphth- 1-yl-2,3-diaza- 1,3,5-heptatriene-1,6-diolato)copper(II) [9], Ni (II)/Co (II) complexes of 3-methoxysalicylaldehyde benzoylhydrazide [10], and polymeric copper(II) complexes of 2- chlorobenzhydrazide [11] were reported. We have investigated the analysis of isonicotinohydrazide [12], furan-2-carbohydrazide monohydrate [13], 4-benzoylpyridine isonicotinyl hydrazone monohydrate [14], benzophenone-2-furoyl hydrazone [15], and (E)-N′-(diphenylmethylene) isonicotinohydrazide dihydrate [16] crystals.

Recently, we have reported a novel Zn(II) complex coordinated with ligands phthalic acid and thiourea [17]. As part of our investigation in the study of Zn(II) phthalate complex, in this study, we report a novel coordination polymer, Zn(II) complex of phthalic acid and hydrazide. It has not been reported as far as our knowledge is concerned. Structural characterization, optical studies, quantification of molecular interactions by finger print plots derived from Hirshfeld surfaces, and theoretical studies of bis(benzene-1,2-dicarboxylato)bis(4-methylbenzohydrazide)zinc are reported in this study.

Experimental

Synthesis

ZPTH was synthesized by mixing AR grade zinc chloride, p-toluichydrazide and phthalic acid in a stoichiometric ratio of 1:2:2 in aqueous medium, stirred for 6 h. The colorless, clear solution was kept at a constant temperature. Crystallization took place in 20–24 days and the crystals were harvested. Optical images of as-grown ZPTH crystals are shown in Supplementary Fig. S1.

$$Zncl_2 + 2CH_3C_6H_4CONHNH_2 + 2 \ C_6H_4(COOH)_2 \xrightarrow[\text{Stirring, 6h}]{\text{Water}}$$

$$[Zn(CH_3C_6H_4CONHNH_2)_2(C_6H_4COO(COOH))_2].$$

Bis(benzene‑1,2‑dicarboxylato)‑
bis(4‑methylbenzohydrazide)zinc (ZPTH)

Characterization techniques

The FT-IR spectrum was recorded using a CARY 630 FT-IR instrument in the range of 400–4000 cm^{-1}. A Bruker AXS (Kappa Apex II) X-ray diffractometer was used for single crystal XRD studies. The powder X-ray diffraction was performed by using Philips Xpert
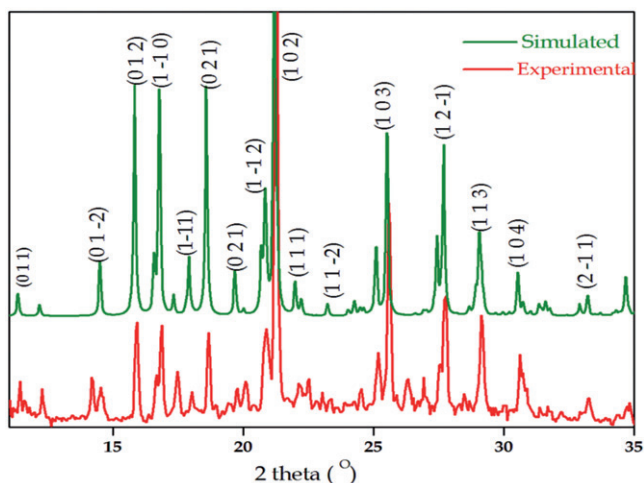
Figure 1. Simulated and experimental powder XRD patterns.

pro triple-axis X-ray diffractometer at room temperature at a wavelength of $1.540\,\text{Å}$ with a step size of $0.0500°$. The samples were examined with CuKα radiation in the 2θ range of $10-80°$. The surface morphologies of the sample were observed using a JEOLSM 5610 LV SEM with the resolution of $3.0\,\text{nm}$, an acceleration voltage range of $0.3-20\,\text{kV}$. The UV–DRS spectra were recorded using Shimadzu UV2600 UV–Vis spectrophotometer. Photoluminescence spectra was recorded by HJY:Fluorolg F3-111 Fluorescence spectrometer. Thermogravimetric (TG) and differential thermal analysis (DTA) were carried out using a NETZSCH STA 449 F3 thermal analyzer in nitrogen atmosphere.

Computational studies

All the theoretical calculations were performed using the GAUSSIAN 09W [18] program package on a personal computer without any constraints on the geometry using density functional group theory (DFT) B3LYP method with LANL2MB as the basis set. Using the GAUSSVIEW 5.0 molecular visualization program [19], the optimized structure of the molecule has been visualized. HOMO and LUMO energies, molecular electrostatic potential (MEP), Mulliken charge population have been computed. Polarizability and first-order molecular hyperpolarizability were calculated by using finite field method as default. Hirshfeld surfaces and fingerprint plots were generated from the crystal data using the CrystalExplorer (Version 3.1), using DFT method with 6-31G(d,p) as basis set [20–23].

Results and discussion

FT-IR

The functional groups are identified by FT-IR spectrum (Supplementary Fig. S2). The hydrazide ligand C=O stretching frequency appears at $1745\,\text{cm}^{-1}$ and carboxylate C=O stretching frequency at $1654\,\text{cm}^{-1}$. An absorption band in the region $3100-3300\,\text{cm}^{-1}$ is due to N–H stretching frequency. The C–O stretching frequency appeared as sharp intensity band around $1205\,\text{cm}^{-1}$. Absorption band appearing at $2986\,\text{cm}^{-1}$ is due to
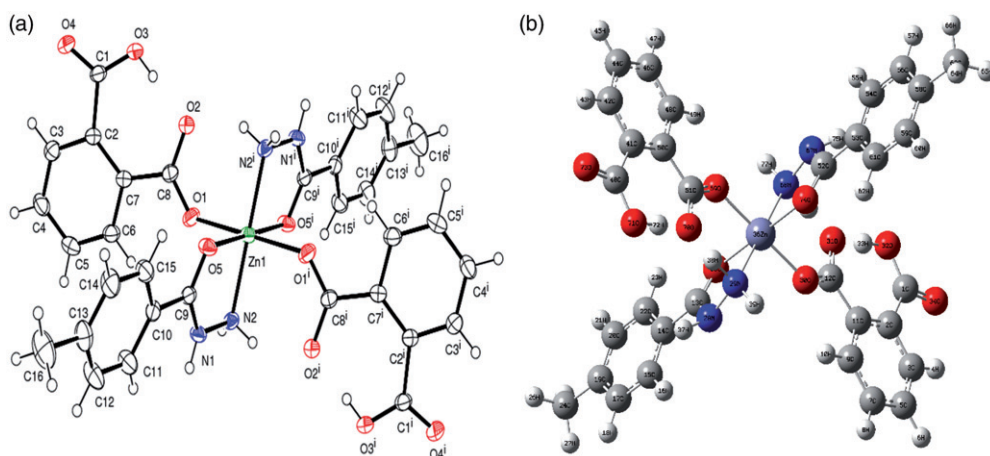
Figure 2. (a) ORTEP (b) Optimized molecular structure of ZPTH.

C–H stretching frequency of aromatic ring. The band at $1555\,\mathrm{cm}^{-1}$ is due to C=C stretching frequency of aromatic region.

Powder XRD

The powder XRD pattern of ZPTH shows that the sample is of single phase without detectable impurity. The well-defined Bragg's peaks at specific 2θ angles show good crystallinity of the material. Peak positions in the powder XRD patterns match with simulated single crystal

XRD pattern with varied intensities. Possibly this could be due to the preferred orientation of the sample used for the diffractogram measurement and the difference in the mosaic spread of the powder and single crystal patterns. High intensity sharp peaks indicate the good crystalline nature of the complex (Fig. 1).

Single crystal XRD

Single crystal XRD shows the refinement of ZPTH in the triclinic system with centrosymmetric P$\bar{1}$ space group. An ORTEP view and optimized molecular structure are shown in Fig. 2. The crystal data and structure refinement parameters are presented in Table 1. The bond lengths, bond angles are listed in Supplementary Table S1 and torsion angles in Supplementary Table S2. The centrosymmetric unit of ZPTH consists of one Zn(II) atom, two phthalate anions, and two p-toluichydrazide ligands with Zn(II) located at the inversion center i. The coordinated sphere around every Zn(II) is a octahedral environment constructed by two oxygen atoms from two partially deprotonated phthalate anions, two nitrogen atoms and two oxygen atoms from two p-toluichydrazide ligands. The carboxylate oxygen-metal bond length is 2.1794(13) Å, whereas Zn–O is equal to 2.0830(12) Å in hydrazide and the N–Zn bond length is 2.0994 (15) Å. The O–Zn–O bond angles range from 87.28(5) to 180.0°. The carboxylate oxygen-carbon bond lengths are, C8-O1 = 1.247(2) and C8-O2 = 1.269(3)Å whereas the hydrazide oxygen-carbon (C9-O5) bond length is equal to 1.251(2) Å. Metal–metal distance across

Table 1. Crystal data and structure refinement.

Crystal data	ZPTH
Empirical formula	$C_{32}H_{30}N_4O_{10}Zn$
Formula weight	695.97
Temperature	296(2) K
Wavelength	0.71073 Å
Crystal system	Triclinic
Space group	$P\bar{1}$
Unit cell dimensions	$a = 5.5275(3)$ Å $\alpha = 94.541(3)°$
	$b = 10.1497(5)$ Å $\beta = 92.174(3)°$
	$c = 14.6095(9)$ Å $\gamma = 104.280(3)°$
Volume	790.41(8) Å^3
Z	1
Density (calculated)	1.462 Mg/m^3
Absorption coefficient	0.841 mm^{-1}
F(000)	360
Crystal size	0.150 x 0.100 x 0.100 mm^3
Theta range for data collection	2.399 to 27.476°
Index ranges	$-7 <= h <= 7, -13 <= k <= 13, -18 <= l <= 18$
Reflections collected	16012
Independent reflections	3597 [R(int) = 0.0367]
Completeness to theta $= 25.242°$	99.90%
Absorption correction	Semi-empirical from equivalents
Max. and min. transmission	0.7455 and 0.6863
Refinement method	Full-matrix least-squares on F^2
Data / restraints / parameters	3597 / 4 / 227
Goodness-of-fit on F^2	1.005
Final R indices [I > 2sigma(I)]	R1 = 0.0326, wR2 = 0.0878
R indices (all data)	R1 = 0.0453, wR2 = 0.0956
Extinction coefficient	n/a
Largest diff. peak and hole	0.244 and -0.223 e.Å^{-3}

Table 2. Hydrogen bonds [Å and °].

D-HA	d(D-H)	d(HA)	d(DA)	< (DHA)
O(3)-H(3A) ... O(2)	0.82	1.58	2.4015(18)	178.7
N(1)-H(1) ... O(4)#2	0.831(15)	1.946(15)	2.763(2)	167(2)
N(2)-H(2A) ... O(2)#1	0.853(14)	2.126(16)	2.853(2)	142.9(18)
N(2)-H(2A) ... O(3)#2	0.853(14)	2.57(2)	3.1091(19)	122.1(17)
N(2)-H(2B) ... O(1)#3	0.835(14)	2.324(17)	3.070(2)	149.0(17)

Symmetry transformations used to generate equivalent atoms: #1 $-x, -y + 1, -z +2$ #2 x, y-1, z #3 $-x + 1, -y +1, -z + 2$.

complex backbone is 5.5275(4)Å. Supplementary Table S3 lists the polyhedral bond lengths and effective coordination number of the system is 5.9152. The polyhedral structure has an average bond length value of 2.1206 Å with a volume of 12.4337 Å^3.

Weak (O–H ….O and N–H ….O) intra- and intermolecular interactions are listed in Table 2. N(1)—H(1) ….O(4) intramolecular hydrogen bond with a bond distance of 2.763(2) Å, and N(2)-H(2A) ….O(3) intermolecular interaction with a bond distance of 3.1091(19) Å are observed. There are only van der Waals interactions between the chain. Strong hydrogen bond is O(3)-H(3A) ….O(2) with a bond distance of 2.4015(18). Three-dimensional perspective of the crystal packing polyhedral structure along the a-, b-, and c—axes are displayed in Supplementary Fig. S3. The optimized molecular structure of ZPTH (Fig. 2b) closely resembles the displacement ellipsoid diagram (Fig. 2a).
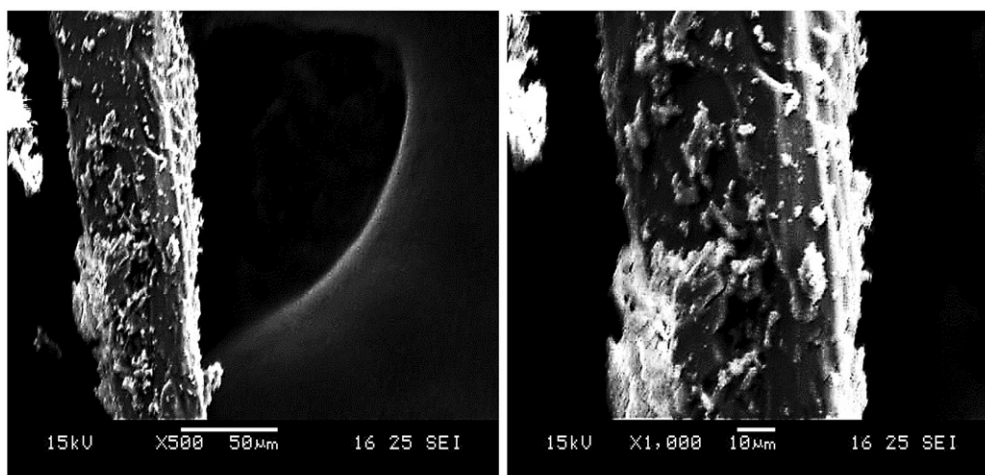
Figure 3. SEM images of ZPTH.

SEM

The SEM micrographs at different magnifications (Fig. 3) give information about the surface morphology revealing the imperfections. The rod like structure exhibits a high surface roughness and defect centers.

UV–Vis–NIR diffuse reflectance spectrum

The UV–visible spectrum of ZPTH reveals high transmittance and the lower cut-off wave length is observed at $\sim$296 nm. The direct band-gap energy of the specimen is estimated as 4.0 eV, from the Tauc plot, $[F(R)h\upsilon]^2$ *versus* hυ (eV) (Fig. 4), where F(R) is Kubelka–Munk function [24] derived from equation,

$$F(R) \;=\; (1 - R)^2/2R \;= Ac/s,$$

R is the reflectance, A is absorbance, c is concentration of the absorbing species and s is scattering coefficient.

Photoluminescence spectrum

Fluorescent emission is exhibited at λ_{max} 401 nm ($\sim$3.09 eV) in the solid state at room temperature (Fig. 5b) under the excitation at 284 nm (Fig. 5a) and it could be due to intraligand fluorescent emission. Phthalic acid exhibits a similar fluorescent emission at λ_{max} 345 nm [25] and a bathochromic shift is observed.

Thermal analysis

Thermogravimetric (TG) analysis and DTA have been carried out simultaneously (Fig. 6) under nitrogen atmosphere at a heating rate 20 K min^{-1} in the temperature range 30–1100 °C. DTA curve shows two endothermic peaks at $\sim$217 and 262 °C
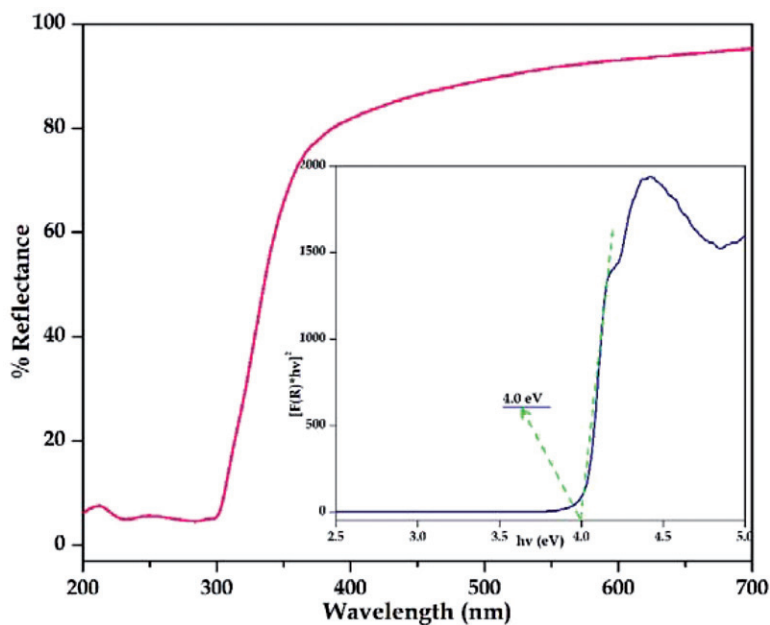
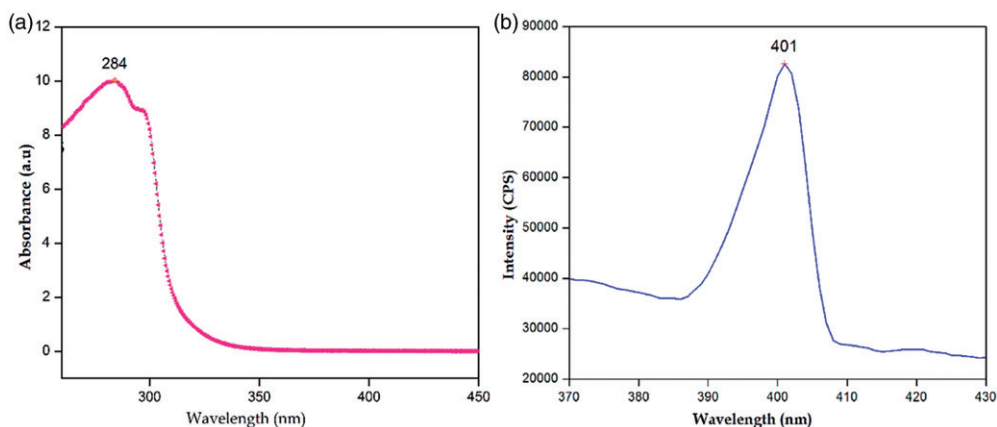**Figure 4.** UV-vis spectrum of ZPTH (Tauc plot is given as an inset).

Figure 5. (a) UV-Vis absorbance spectrum (b) Photoluminescence emission spectrum of ZPTH in the solid state at room temperature.

corresponding to the decomposition of ZPTH. The TGA curve shows weight loss in the range 175–800 °C, attributed to the decomposition of coordinated hydrazide and phthalate ligands. It is observed that the ZPTH is stable up to 175 °C. There is no decomposition up to the melting point showing the stability.

First-order molecular hyperpolarizability

Calculated polarizability (α), first-order molecular hyperpolarizability (β) and dipole moment (μ) of the specimen are, 169.8229×10^{-24} esu, 1.6529×10^{-33} esu and 0.0026 D,
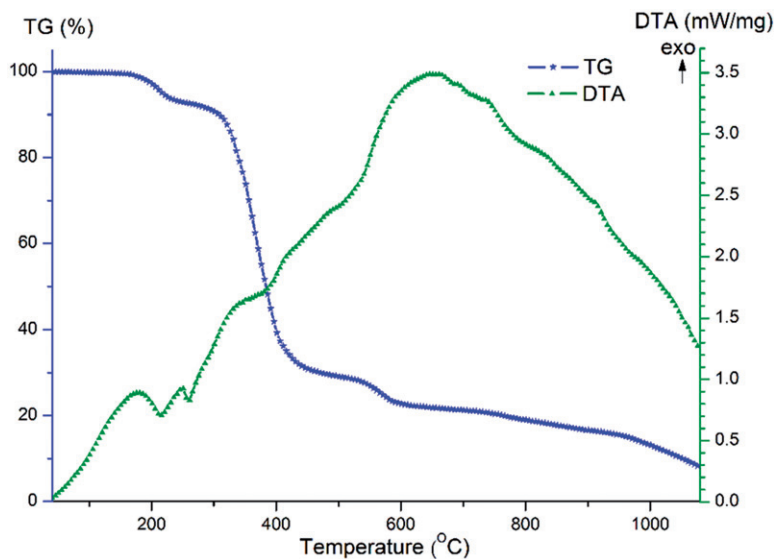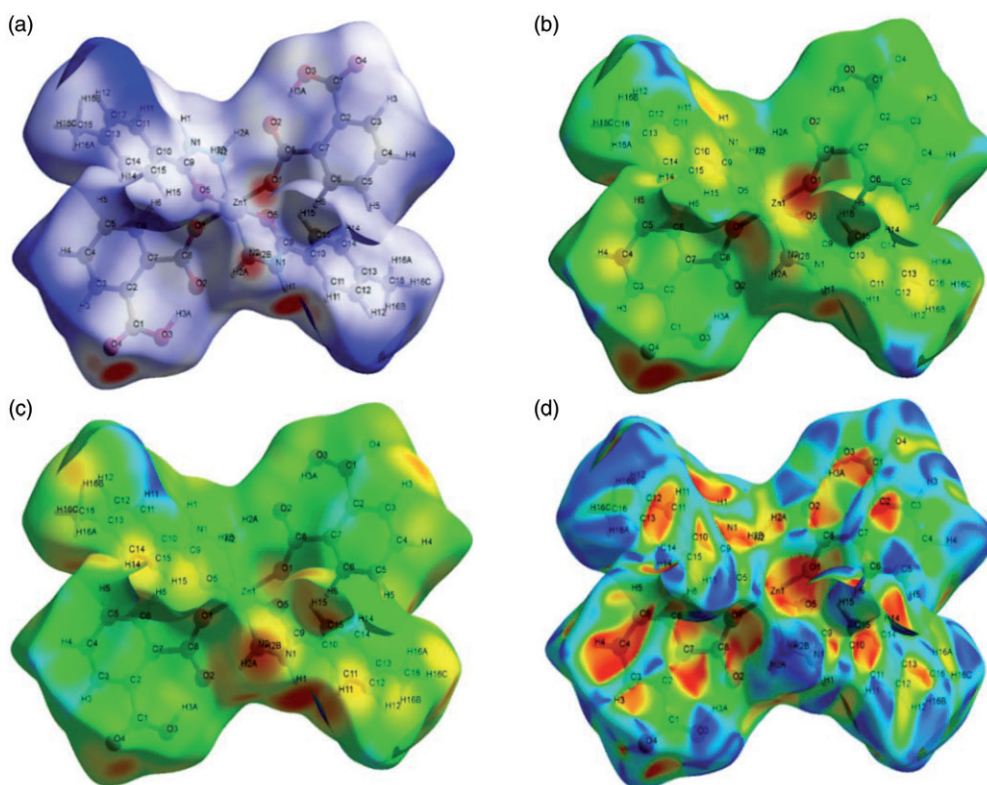
Figure 6. TG/DTA of ZPTH.

Figure 7. Hirshfeld surfaces of ZPTH (a) d_{norm}, (b) d_e, (c) d_i, and (d) shape index.
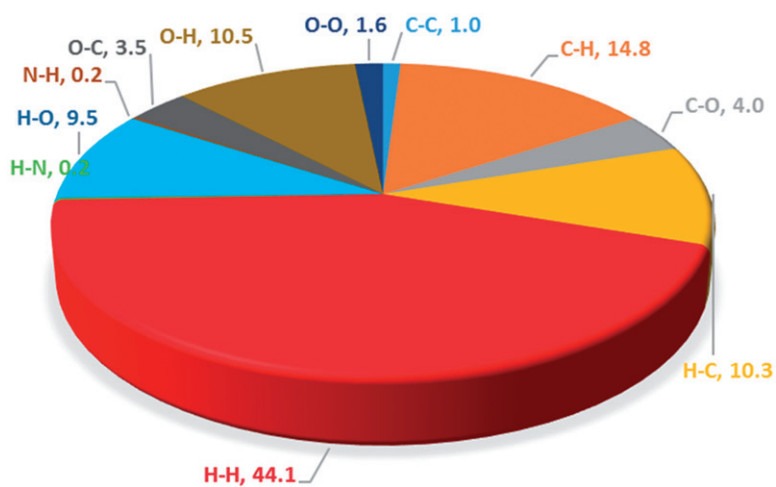
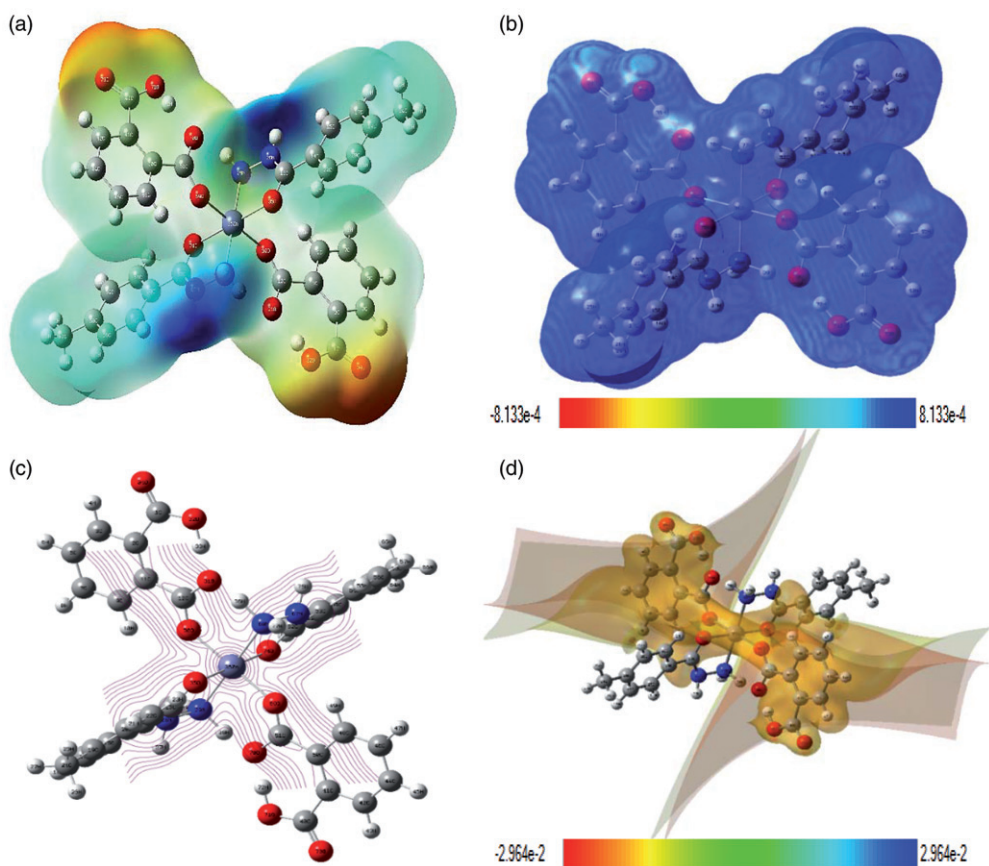**Figure 8.** Quantities of molecular interactions represented in a pie chart.

Figure 9. Electron density surface (a) MEP, (b) total electron density, (c) electron contour, and (d) ESP.
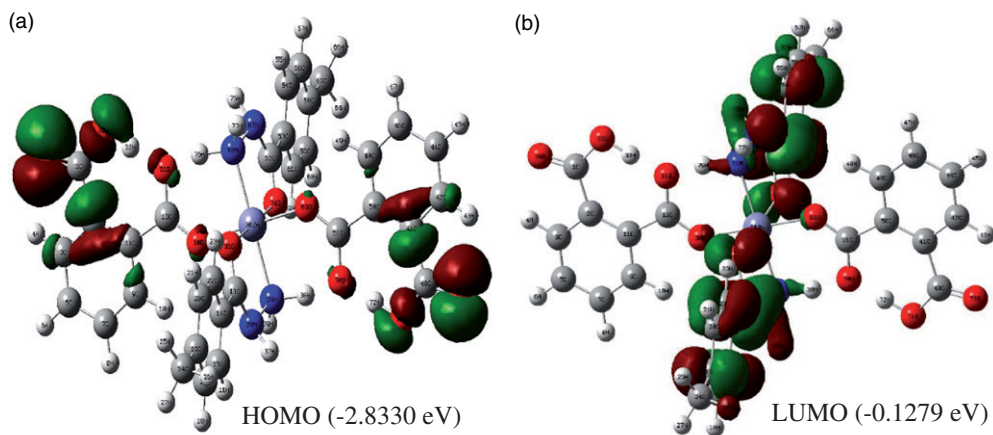
(a)

(b)

HOMO (-2.8330 eV)   LUMO (-0.1279 eV)

Figure 10. (a) HOMO and (b) LUMO of ZPTH.

respectively (Supplementary Table S4). Interestingly, β value of bis(benzene-1,2-dicarboxylato)bis(thiourea)zinc [17], ($C_{18}H_{18}N_4O_8S_2Zn$) is estimated as 6.1375×10^{-30} esu ($\sim$31.5 times of urea: $\sim$3700 times of ZPTH) and $\mu = 17.1437$ D. Negligible microlevel nonlinearity in the case of title compound in comparison could be attributed to packing and orientation cancelling charge transfer leading to the absence of NLO response. Literature survey of reported transition metal hydrazide complexes (Supplementary Table S5) clearly reveals that mostly they crystallize centrosymmetrically.

Hirshfeld surface analysis

The Hirshfeld surface was derived using the data obtained from single crystal XRD analysis. The normalized contact distance d_{norm} is based on d_e and d_i representing the distances of the nearest nucleus external and internal to the surface respectively. The shape index indicates the shape of the electron density surface around the molecular interactions. The visible deep red circular depressions indicate hydrogen bonding contacts (Fig. 7a–c) and bright red areas in surface plot indicate O…H and H…O dominant interactions. The small light color range areas represent the weaker and longer contacts.

Quantification of all intra- and intermolecular interactions are displayed as a pie chart Fig. 8 and fingerprint plots shown in Supplementary Fig. S4. A spike in the lower left area represents O…H interactions whereas right region represents the H…O interactions. Strong interactions are, H…H, C…H, H…C, O…H, and H…O and weak interactions are, O…O, C…O, O…C, N…H, H…N, and C…C.

Molecular electrostatic potential

Negative regions of MEPs are for the electrophiles (red) and the positive MEPs are for nucleophiles (blue). In MEP, light green region corresponds to the halfway. These potential surfaces give an idea about the net electrostatic effect produced by the total charge distribution of atom or molecule. Electrostatic potential maps and electron densities of MEPs are displayed in Fig. 9.

Mulliken population analysis

Mulliken atomic charges are calculated by determining the electron population of each atom as defined by the basis function (Supplementary Table S6). Supplementary Fig. S5 shows the Mulliken atomic charge distribution and Mulliken plot of $[Zn(C_6H_4COO(COOH))_2(CH_3C_6H_4CONHNH_2)_2]$. All the oxygen and nitrogen atoms have a negative charge and behaved as electron donors. Carbon atoms (C2, C3, C5, C7, C9, C11, C14, C15, C17, C20, C22 C24, C41, C42, C44, C46, C48, C50, C53, C54, C56, C59, C61, and C63) have negative charge. All the remaining atoms and carbon atoms (C1, C12, C13, C19, C40, C51, C52, and C58) are positive.

Frontier molecular orbital analysis (FMO)

The frontier orbital gap facilitates in characterizing the chemical reactivity and kinetic stability of the molecule. Fig. 10 displays the highest occupied molecular orbital (HOMO) and lowest unoccupied molecular orbital (LUMO), calculated using B3LYP/LANL2MB as basis set. The HOMO is the orbital that primarily plays as an electron donor and the LUMO is the orbital that mainly plays as an electron acceptor.

Conclusions

Single crystals of a novel Zn(II) complex, bis(benzene 1,2-dicarboxylato)bis(4-methylbenzo-hydrazide)zinc were successfully grown and characterized. The presence of the functional groups has been identified by FT-IR spectroscopic technique. The X-ray diffraction study confirms the crystal structure and crystallinity of the grown crystal. The band gap energy of this complex is 4.0 eV as estimated from the optical reflectance spectrum. Fluorescent emission studies indicate that this complex is a promising photoactive material. The material has a good thermal stability as revealed by thermal pattern. Negligible beta value and centrosymmetric crystallization rule out NLO responses. The two-dimensional fingerprint plots give an idea about intermolecular interaction patterns and as revealed H….H, C….H and O….H interactions are predominant whereas O….O, C….O, N….H and C….C interactions are weak. Noncovalent forces are mainly responsible for crystal cohesion. Electron delocalization is confirmed by MEP, ESP, and total electron density, Mulliken population analysis reveals the intermolecular charge transfer present in the complex system. Further research is underway to synthesize novel transition metal complexes of phthalic acid and other ligands and comparison of properties will reveal interesting insights.

Funding

Supplementary material

Crystallographic data of ZPTH has been deposited with the Cambridge Crystallographic Data Centre [CCDC 1583827]. Copies of the data can be obtained free of charge at

www.ccdc.cam.ac.uk/ conts/retrieving.html or from the Cambridge Crystallographic Data Centre (CCDC), 12 Union Road, Cambridge CB2 1EZ, UK; fax: +4401223 336 033; email: deposit@ccdc.cam.ac.uk.

References

[1]   Mihalcea, I., Henry, N., & Loiseau, T. (2011). *Cryst. Growth Des.*, *11*, 1940.
[2]   Pouralimardan, O., Chamayou, A.-C., Janiak, C., & Hosseini-Monfared, H. (2007). *Inorg. Chim. Acta.*, *360*, 1599.
[3]   Gull, P., & Hashmi, A. A. (2015). *J. Braz. Chem. Soc.*, *26*, 1331.
[4]   Shankar, M. V., & Varma, K. B. R. (1996). *Ferroelectr. Lett. Sec.*, *21*, 55.
[5]   Miniewicz, A., & Bartkiewicz, S. (1993). *Adv. Mater. Opt. Electron.*, *2*, 157.
[6]   Neto, B. A. D., Viana, B. F. L., Rodrigues, T. S., Lalli, P. M., Eberlin, M. N., da Silva, W. A., et al. (2013). *Dalton Trans. 42*, 11497.
[7]   Zhou, Y.-X., Yuan, R.-F., Fan, C.-L., Liu, L.-E., Wu, B.-L., & Zhang, H.-Y. (2012). *J. Coord. Chem.*, *65*, 3133.
[8]   Ienco, A., Mealli, C., & Dodoff, N. I. (2002). *Z. Naturforsch.*, *57b*, 865.
[9]   Fazlic, R., Divjakovic, V., Leovac, V. M., & Chundak, S. Y. (1991). *Acta Cryst. C47*, 714.
[10] Zou, L.-F., Yang, X.-Y., Wang, D.-X., Gao, Y., Wang, Y., & Li, Y.-H. (2012). *Asian J. Chem. 24*, 2909.
[11] Paixão, D. A., de Oliveira, L. P., Maia, P. I. da S., Deflon, V. M., Carneiro, Z. A., de Almeida, K. J., et al. (2018). *J. Saudi Chem. Soc.*, doi:10.1016/j.jscs.2018.01.002.
[12] Meenatchi, V., & Meenakshisundaram, S. P. (2015). *RSC Adv.*, *5*, 64180.
[13] Meenatchi, V., Agilandeshwari, R., & Meenakshisundaram, S. P. (2015). *RSC Adv.*, *5*, 71076.
[14] Meenatchi, V., Muthu, K., Rajasekar, M., & Meenakshisundaram, S. P. (2014). *Spectrochim. Acta. Part A*, *124*, 423.
[15] Meenatchi, V, Muthu, K., Rajasekar, M., & Meenakshisundaram, S. P. (2014). *Optik.*, *125*, 4196.
[16] Meenatchi, V., Muthu, K., Rajasekar, M., Bhagavannarayana, G., & Meenakshisundaram, S. P. (2014). *Optik.*, *125*, 4181.
[17] Balakrishnan, C., Sivaraman, S., Manonmani, M., Markkandan, R., Meenakshisundaram, S. P., & Sockalingam, R. M. (2018). *Mol. Cryst. Liquid Cryst.*, *664*, 182–194. doi:10.1080/15421406.2018.1467097.
[18] Frisch, M. J., Trucks, G. W., Schlegel, H. B., Scuseria, G. E., Robb, M. A., & Cheeseman, J. R., et al. (2009). *Gaussian09, Revision C.01*, Wallingford, CT: Gaussian, Inc.
[19] Dennington, R., Keith, T., & Millam, J. (2009). *GaussView, Version 5*, Shawnee Mission, KS: Semichem Inc.
[20] Spackman, M. A., & Jayatilaka, D. (2009). *Cryst. Eng. Commun. 11*, 19.
[21] Hirshfeld, F. L. (1977). *Theoret. Chim. Acta (Berl.)*. *44*, 129.
[22] Wolff, S. K., Grimwood, D. J., McKinnon, J. J., Turner, M. J., Jayatilaka, D., & Spackman, M. A. (2012). *CrystalExplorer (Version 3.1)*, Crawley, WA: University of Western Australia.
[23] Spackman, M. A., & McKinnon, J. J. (2002). *Cryst. Eng. Commun.*, *4*, 378.
[24] Kubelka, P., & Munk, F. (1931). *Z. Tech. Phys. 12*, 593.
[25] Wang, S., Hou, Y., Wang, E., Li, Y., Xu, L., Peng, J., et al. (2003). *New J. Chem. 27*, 1144.